DESIGN AND PERFORMANCE ANALYSIS OF AN IN-WHEEL HUB REDUCER

UDC:621.833.6
Original scientific paper https://doi.org/10.46793/adeletters.2022.1.4.1

Milan Vasić[1*], Mirko Blagojević[2], Boris Stojić[3], Samir Dizdar[4]

[1] Academy of Applied Technical Studies Belgrade, College of Applied Engineering Sciences in Pozarevac, Belgrade, Serbia
[2] University of Kragujevac, Faculty of Engineering, Kragujevac, Serbia
[3] University of Novi Sad, Faculty of Technical Sciences, Novi Sad, Serbia
[4] Berdiz Consulting AB, Gothenburg, Sweden

Abstract:
In order to reduce the greenhouse effect caused by CO_2 emissions, a lot of car manufacturers are developing battery electric vehicles (BEVs). Almost all of these vehicles have a traditional powertrain layout with the drive unit located in the car body. However, in recent years, a new technology called in-wheel motors has appeared. It significantly improves handling and manoeuvrability of vehicles but it also presents a challenge for both researchers and manufacturers. Since the motors are fitted into a limited space, they must provide high torque and high efficiency. When a reducer is used, the amount of torque needed is decreased several times, hence the overall dimensions of the motor are reduced. This paper studies a number of issues such as the basic concepts of the in-wheel hub drive systems, traction balance, preliminary gear ratio and possible design solutions for reducers used in in-wheel hub drive units. Characteristics of single-stage planetary and cycloidal reducers are analysed in detail. The results show that planetary reducers have an advantage if a lower gear ratio is needed.

ARTICLE HISTORY
Received: 11.08.2022.
Accepted: 21.11.2022.
Available: 31.12.2022.

KEYWORDS
In-wheel hub motors, transmission configuration synthesis, planetary drive, cycloid drive, overall dimensions, efficiency, gear ratio

1. INTRODUCTION

The global impact of conventional road transport is entangled with different kinds of problems such as negative effects on the environment and climate, resource depletion and rising prices of fossil fuels. Efforts to reduce these negative effects accompanied by requirements of national and international regulations forced the automotive industry to develop and promote more energy and environmentally efficient concepts of how to power road vehicles. Due to these tendencies, research and development activities have been intensified in the field of hybrid electric vehicles (HEVs), fuel cell vehicles (FCVs) and battery electric vehicles (BEVs), hence numerous researchers have been engaged in developing transmission [1,2], suspension systems [3,4] electric motors [5,6], in generation of driving cycles [2,7] and in studies related to other areas of automotive engineering.

One of the important design features of electric motors is their ability to be fitted directly in the drive wheels (IWM). The main advantages of this concept include a potential to improve the dynamic performance of the vehicle due to a more favourable mass distribution, the absence of need for complex transmission, greater flexibility in the use of available space [8,9], etc. That is why this type of drive concept is in the focus of research.

Development of permanent magnet synchronous motors (PMSM) made it possible to have a direct drive without a gearbox. These motors provide higher torque and higher efficiency compared to induction motors (IM) [10].

Although power losses in power transmission generally occur when reducers are used, the reducers with one or two gear pairs are far more

*CONTACT: Milan Vasić, e-mail: mvasic@atssb.edu.rs

efficient than the complex multi-stage gearboxes used in vehicles with IC engines. Furthermore, a reducer decreases the amount of torque that needs to be generated, which in turn reduces the overall dimensions of the motor.

Unlike conventional electric cars with the drive located in the car body, where a single-stage and two-stage planetary reducers or reducers with parallel shafts [11] are generally used, in the in-wheel hub drives, planetary [12,13] and cycloidal reducers [14,15] or their combinations with involute external gears are mainly used.

In recent decades, these reducers have been the subject of intensive research. Researchers have dealt with dynamic load analysis [16-18], stress-strain analysis [19,20], determination of efficiency [21,22], thermal analysis [23,24] and with many other issues.

The aim of this paper is to perform a comparative analysis of the basic characteristics of planetary and cycloidal reducers used in in-wheel-hub drives. The analysis was performed in the MATLAB software package, in which the presented models were implemented.

2. BASIC CONCEPTS AND COMPONENTS OF THE IWM DRIVE UNIT

IWM drive units can be installed in the non-drive wheels of hybrid electric vehicles (HEVs) to enable four-wheel drive (4WD), in the rear or the two front wheels of smaller electric vehicles (2 IWM), or in the front and rear wheels of larger vehicles (4 IWM) (Fig. 1).

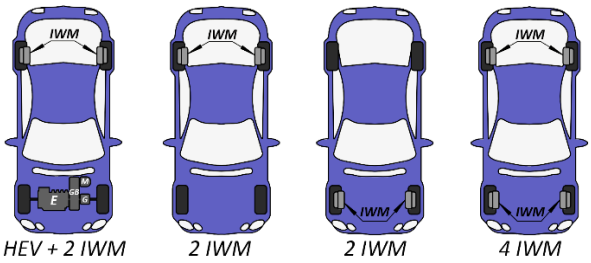

Fig. 1. Possible applications of IWM drive units

Basically, the drive unit of the in-wheel hub system consists of an electric motor, a reducer and a wheel hub (Fig. 2). The main elements of the electric motor are the stator, which is attached to the non-rotating housing, and the rotor, which is connected by a shaft to the sun gear in planetary reducers or to the input eccentric shaft in cycloidal reducers.

In order to ensure active cooling of the housing, i.e. of the stator and lubricating oil, there are heat dissipation fins on its outer surface.

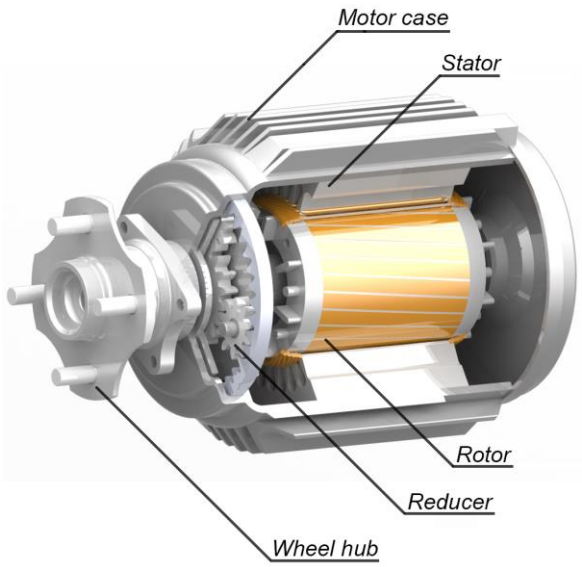

Fig. 2. Basic components of an IWM drive unit

3. TRACTION BALANCE, TORQUES AND MOMENTS OF INERTIA

A vehicle moving at a constant speed is opposed by: the rolling resistance (F_r), aerodynamic drag (F_{DF}), grading resistance (F_g), and, when moving at non-stationary speeds, by inertial forces (Fig. 3).

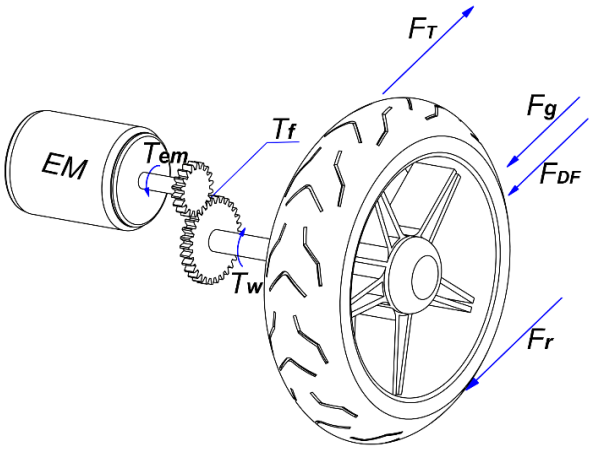

Fig. 3. Drivetrain loading

According to Newton's second law, the traction balance equation can be written as [25,26]:

$$m \cdot \frac{dv(t)}{dt} = N_{dw} \cdot F_T(\omega_{em}) - \\ -\left[F_r(t) + F_{DF}(t) + F_g(t)\right] \quad (1)$$

where: m – effective mass, (Kg) ; $dv(t)/dt$ – change in speed per unit of time – acceleration, (m/s^2); N_{dw} – number of drive wheels; $F_T(\omega_{em})$ – tractive effort as a function of the motor angular velocity, (N).

The effective mass (m) consists of the actual translational mass of the vehicle (m_v) carrying capacity (m_c) and the equivalent masses of the moments of inertia of rotating elements such as wheels(m_w) and motor rotors (m_{em}), whereby the values of the other equivalent masses are neglected [25].

$$m = m_v + m_c + m_{em} + m_w \tag{2}$$

The equivalent mass of the moment of inertia of the motor rotor can be determined using the following expression [26]:

$$m_{em} = \frac{J_{em} \cdot {u_R}^2 \cdot N_{dw} \cdot \eta_{em} \cdot \eta_R}{{r_{dyn}}^2} \tag{3}$$

where: J_{em} – moment of inertia of the electric motor, (kg/m^2); u_R – gear ratio of the reducer; η_{em} – motor efficiency; η_R – reducer efficiency; r_{dyn} – effective radius of the tire, (m).

The equivalent mass of the moment of inertia of the wheels can be determined as [26]:

$$m_w = \frac{J_w \cdot N_w}{{r_{dyn}}^2} \tag{4}$$

where: J_w – moment of inertia of a wheel, (kg/m^2); N_w – total number of wheels.

The rolling resistance can be determined based on the expression [25,26]:

$$F_r(t) = m_{vc} \cdot g \cdot \mu_r \cdot cos(\alpha) \tag{5}$$

where: μ_r – rolling resistance coefficient; α – road grade angle, (°); g – acceleration of gravity, (m/s^2); m_{vc} – translational mass of the vehicle increased by the carrying capacity, (kg);

The rolling resistance coefficient of the wheels, which is a function of the velocity of the vehicle, can be determined using the expression [26]:

$$\mu_r = \mu_0 \cdot \left(1 + \frac{v(t)}{161}\right) \tag{6}$$

where: μ_0 – rolling resistance coefficient for the velocity up to 60 km/h (for the smooth tarmac road $\mu_0 = 0.01$; for the smooth concrete road $\mu_0 = 0.011$; for the rough, good concrete surface $\mu_0 = 0.014$; for the good stone paving $\mu_0 = 0.020$; for the bad, worn road surface $\mu_0 = 0.035$) [25]; $v(t)$ – current speed of the vehicle.

The aerodynamic drag is defined as [25,26]:

$$F_{DF}(t) = \frac{1}{2} \cdot \rho_{air} \cdot C_d \cdot A_f \cdot \left(\frac{v(t)}{3.6}\right)^2 \tag{7}$$

where: ρ_{air} – air density, (kg/m^3); A_f – vehicle frontal area, $A_f = 0{,}82 \cdot b_v \cdot h_v$, (m^2) ; b_v – maximum vehicle width, (m); h_v – maximum vehicle height, (m); C_d – aerodynamic drag coefficient which depends on the outer shape of the vehicle and the Reynolds number. The typical value of this coefficient ranges from 0.18 for a perfect aerodynamic body to 0.25÷0.30 when tangential resistances and surface discontinuity resistances are included [25].

The grading resistance can be determined based on the expression [25,26]:

$$F_g(t) = m_{vc} \cdot g \cdot sin(\alpha) \tag{8}$$

The current value of the torque on the wheel can be defined as:

$$T_w(t) = \frac{\left[F_r(t) + F_{DF}(t) + F_g(t) + m \cdot \frac{dv(t)}{dt}\right] \cdot r_{dyn}}{N_{dw}} \tag{9}$$

The tractive effort that the motor can provide depends on the motor characteristics and it can be defined as:

$$F_T(\omega_{em}) = \left[T_{em}(\omega_{em}) - T_f\right] \cdot \frac{u_R}{r_{dyn}} \tag{10}$$

where je: $T_{em}(\omega_{em})$ – torque which depends on the current speed of the motor, (Nm) ; T_f – total friction torque in reducers, (Nm).

4. SELECTION OF A REDUCER

It is well known that a reducer significantly decreases the torque that needs to be produced.

Apart from the direct drive (Fig. 4.a), the torque from the motor can be transmitted to the wheel using:

- a single-stage reducer with involute external gears (Fig. 4.b);
- a single-stage reducer with involute internal and external gears (Fig. 4.c);
- a single-stage planetary reducer (Fig. 4.d);
- a single-stage planetary reducer with double planet gears (Fig. 4.e);
- a single-stage cycloidal reducer (Fig. 4.f);
- a two-stage reducer with involute external gears (Fig. 4.g);
- a two-stage reducer with involute external gears in the first stage and planetary or cycloidal gears in the second gear stage (Fig. 4.h, and j).

Reducers with drive shafts above the wheel axis (Fig. 4.b, c, g, h, i) are mainly used when a greater distance from the ground is needed, hence such reducers are generally found in off-road vehicles.

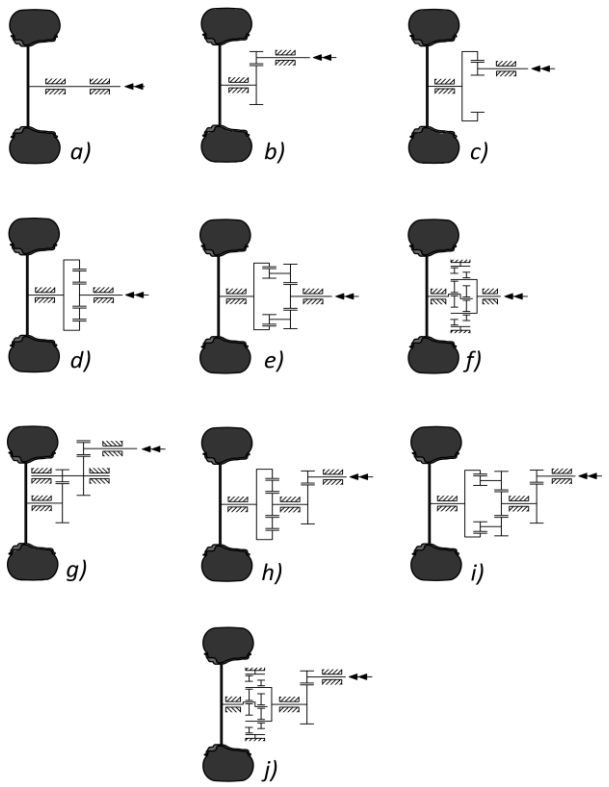

Fig. 4. Schematic presentation of the reducer in the in-wheel hub drive

4.1 Gear ratio of the reducer

The speed of a vehicle at a given speed of the motor can be considered a preliminary criterion for the selection of the gear ratio of the reducer [27,28].

$$u_R = \frac{0.377 \cdot n_{max} \cdot r_{dyn}}{v_{max}} \qquad (11)$$

where: n_{max} – maximum speed of the motor, (min^{-1}); v_{max} – maximum speed of the vehicle, (km/h);

In addition, the gear ratio can also be adopted based on the criterion of the ability to realize the driving force needed to overcome the grade of the road at the maximum torque of the motor, or based on the criterion of the maximum available adhesion force [27,28].

In general, single-stage planetary reducers are limited to a gear ratio of 10:1. Above this gear ratio, they become inefficient (large overall dimensions and high price), so it is more practical to increase the number of gear stages to two. Yet another limitation occurs at small gear ratios from 4 to 1, because of a small module and problems in its manufacture [29].

The gear ratio for one gear stage of a cycloidal reducer equals the number of the cycloid disc teeth $(u_{CR} = z_1)$. This feature allows cycloidal reducers to achieve much higher values of gear ratios compared to planetary reducers. For a single-stage cycloidal reducer, the gear ratio ranges from 3 to 119 [30].

However, cycloidal reducers, as power transmissions of a newer generation, require very precise manufacturing, especially when it comes to their essential elements such as a cycloidal gear.

4.2 Average loads

Load and dynamic behaviour analysis of reducer elements is a very complex task which can be realised in several ways.

In real conditions, loads acting on a moving vehicle are not of constant intensity and of idealised sinusoidal shape, they are random and change depending on the driver's preferences and road conditions.

Therefore, in order to evaluate the reliability and durability of the reducer components under random load, it is necessary to collect load signals and create a driving cycle. Since there are different road conditions in different areas, data is collected for city driving conditions, local road driving conditions, mountain road driving conditions and high speed driving conditions [2].

This paper uses a simplified version of *The Worldwide Harmonised Light Vehicles Test Procedure Cycle* (WLTP cycle) [31] which has been used to determine fuel consumption and exhaust gas emissions for all passenger vehicles since 2017. The duration of the cycle is 30 min, the average speed of the vehicle is 46.6 km/h, and the maximum speed is 131 km/h. Vehicle speed and motor torque as a function of time are presented in Fig. 5 and 6.

In order to define the relevant load, in addition to the load spectrum that shows how many times the reducer works under the nominal and less than nominal torque [32], simplified statistical parameters such as average, maximum and minimum values can be used for preliminary results [33].

The average torque of the input shaft can be obtained using the expression [33]:

$$T_{em} = \sqrt[\frac{10}{3}]{\frac{t_1 \cdot n_1 \cdot T_1^{\frac{10}{3}} + \cdots + t_i \cdot n_i \cdot T_i^{\frac{10}{3}}}{t_1 \cdot n_1 + \cdots + t_i \cdot n_i}} \qquad (12)$$

where: T_i – motor torque, (Nm); n_i –motor speed, (min^{-1}); t_i – amplitude duration time; (s).

The average speed of the input shaft is given by the expression [33]:

$$n_{em} = \frac{t_1 \cdot n_1 + \cdots + t_i \cdot n_i}{t_1 + \cdots + t_i} \quad (13)$$

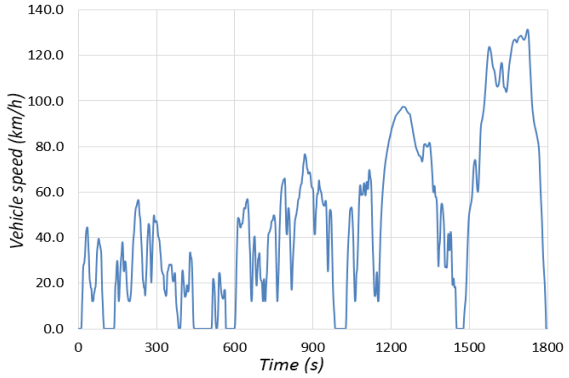

Fig. 5. Vehicle speed as a function of time [31]

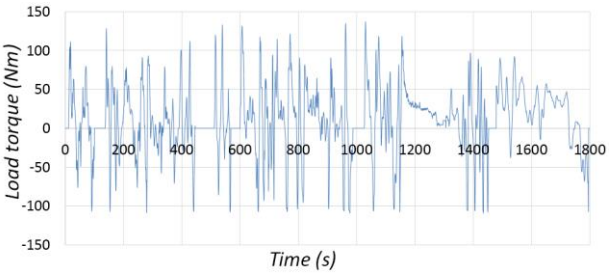

Fig. 6. Vehicle motor torque as a function of time

4.3 Dimensions

Since motors with reducers are mounted in all wheels, their length in direction of the axle should be kept as short as possible, while their diameter is limited by the inner diameter of the wheel.

Dimensions of the planetary reducer primarily depend on the gear ratio ($\boldsymbol{u_R}$), the module ($\boldsymbol{m}$) and the number of gear teeth $(\boldsymbol{z_a}, \boldsymbol{z_b}, \boldsymbol{z_g})$, as shown in Fig. 7.

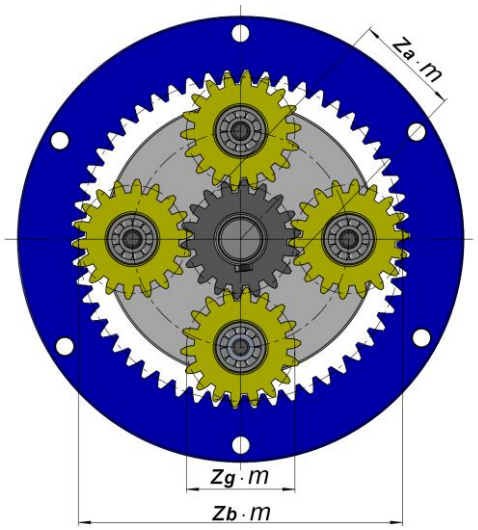

Fig. 7. Dimensions of the main elements of the planetary reducer

The basic design relations between the number of teeth and the number of planet gears are as follows [34]:

$$z_b = z_a + 2z_g \quad (14)$$

$$\frac{z_a + z_b}{N} = Integer \quad (15)$$

$$z_g + 2 < (z_b - z_g) \cdot sin\left(\frac{\pi}{N}\right) \quad (16)$$

where: $\boldsymbol{z_a}$ – number of sun gear teeth; $\boldsymbol{z_g}$ – number of planet gear teeth; $\boldsymbol{z_b}$ – number of ring gear teeth; $\boldsymbol{N}$ – number of planet gears.

Dimensions of the cycloidal reducer depend on the size of the cycloid disk (Fig. 8), whose profile is generated based on the equations [35]:

$$\begin{aligned} x &= r \cdot cos(\alpha) + e \cdot cos(\alpha + \beta) - \\ &\quad - \frac{D_0}{2} \cdot cos(\alpha + \phi) \\ y &= r \cdot sin(\alpha) + e \cdot sin(\alpha + \beta) - \\ &\quad - \frac{D_0}{2} \cdot sin(\alpha + \phi) \end{aligned} \quad (17)$$

where: r – radius of the pitch circle of the ring gear rollers, (mm); e – eccentricity, (mm); D_0 – ring gear roller diameter, (mm); β – drive angle, (°).

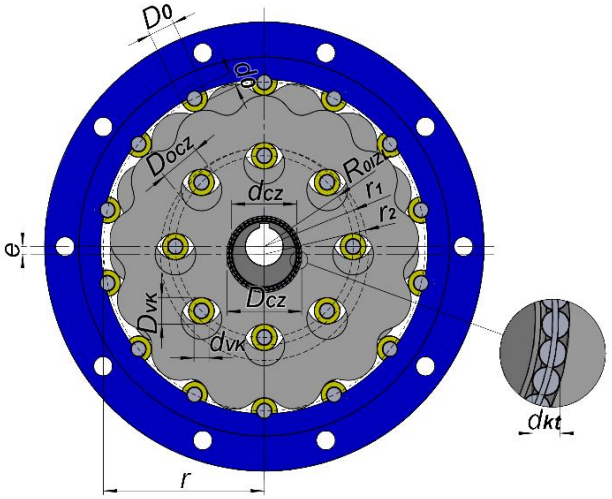

Fig. 8. Dimensions of the main elements of the cycloidal reducer

The values of the angles α and ϕ are given by the expression [35]:

$$\alpha = \frac{1}{u_R} \cdot \beta \quad (18)$$

$$\phi = arctan\left[\frac{sin(\beta)}{\frac{r}{e \cdot z_2} + cos(\beta)}\right] \quad (19)$$

where: $\boldsymbol{z_2}$ – number of ring gear rollers.

4.4 Efficiency of the reducer

Efficiency is defined as the ratio of input and output power and it depends on the amount of lost energy. In general, power losses in reducers can be divided into load-independent and load-dependent losses. Load-independent losses are mainly related to the lubricant and the shaft sealing. Load-dependent losses are the result of friction in the contact of power transmission components and rotary motion components. This primarily refers to the contact of the teeth of the sun gear, the planet gear and the internal ring gear in the planetary reducer, the contact between the cycloid disc teeth and the ring gear rollers, between the output rollers and holes in the cycloid disc, between the elements of the rolling bearings, as well as the contact between the rollers and their pins in cycloidal reducers.

As a result of many years of research, numerous models are now available to predict the efficiency. Certain models take into account the friction that occurs in meshing and supports and are based on the calculation of forces and external loads [21,22]. However, it is quite complex and often unreliable to determine the efficiency using such models because there is a small amount of reliable information about the actual values of the friction coefficient. Other models are based on the assumption that the forces acting on the reducer elements do not change during rotation, hence their relations can be expressed through efficiency of fixed axes transmissions [34,36]. It is obvious that the latter method is more or less approximate because it does not take into account the losses in the lubricant, which are almost impossible to determine due to the complex configuration of the reducer components. These power losses, which depend on the type of reducer and the configuration of its elements, can be determined more accurately only experimentally.

4.4.1 Efficiency of the planetary reducer

If only the power losses that occur in meshing and the losses in the planet gear bearings are considered, the efficiency for a planetary reducer with an internal ring gear (Fig. 7) can be determined using the expressions defined by Kudryavcev [36]:

$$\eta_{PR} = 1 - \frac{z_b}{z_a + z_b} \cdot \psi_{P_{loss}} \qquad (20)$$

where: $\psi_{P_{loss}}$ – power loss coefficient of the planetary reducer.

The power loss coefficient $\left(\psi_{P_{loss}}\right)$ is equal to the sum of coefficients of power loss in meshing (ψ_c) and the sum of coefficients of power loss in the planet gear bearings (ψ_b), i.e.:

$$\psi_{P_{loss}} = \psi_c + \sum_j \psi_b \qquad (21)$$

where: j – number of the planet gear bearings.

Since power branching from the ring gear to several planet gears does not affect meshing losses, only one power flow is used to determine the meshing coefficient (ψ_c) [34]. The modern technical literature recommends several expressions to get its approximate value. One of the most common expressions that takes into account both internal and external meshing is the following [34,36]:

$$\psi_c = 2.3 \cdot \mu_p \cdot \left[\left(\frac{1}{z_a} + \frac{1}{z_g}\right) + \left(\frac{1}{z_g} - \frac{1}{z_b}\right)\right] \qquad (22)$$

where: μ_p – coefficient of friction on the teeth flanks.

The value of the coefficient of friction on the teeth flanks $\left(\mu_p = 1.25 \cdot f_p\right)$ depends on the sum of circumferential velocities at meshing $v_\Sigma = (v_1 + v_2) \cdot sin(\alpha_{wt})$ [36].

The value of the coefficient of power loss in the rolling bearings (ψ_b) is determined as:

$$\psi_b = \frac{T_{fp}}{T_{pg}} \qquad (23)$$

where: T_{fp} – friction torque in the bearing, (Nm); T_{pg} – planet gear torque, (Nm).

The approximate value of the friction torque in the bearing T_{fp} is given by the expression:

$$T_{fp} = 0{,}5 \cdot \mu_b \cdot F_r \cdot d_{in} \cdot 10^{-3} \qquad (24)$$

where: μ_b – friction coefficient in the bearing; F_r – radial load of the bearing, (N); d_{in} – inner diameter of the bearing, (mm).

4.4.2 Efficiency of the cycloidal reducer

If only the power losses that occur in meshing of the rollers and the cycloid disc and the losses in the cycloid disc bearings are considered, the efficiency of the cycloidal reducer, shown in Fig. 8, can be determined using the expression also defined by Kudryavcev [36]:

$$\eta_{CR} = \frac{1 - \psi_{C_{loss}}}{1 + z_1 \cdot \psi_{C_{loss}}} \qquad (25)$$

where: z_1 – number of the cycloid disc teeth; $\psi_{C_{loss}}$ – coefficient of the cycloidal reducer power loss.

The coefficient of the cycloidal reducer power loss $(\psi_{C_{loss}})$ equals the sum of the coefficient of power loss due to friction between the ring gear rollers and the cycloid disc teeth (ψ_1), coefficient of power loss between the output rollers and the holes in the cycloid disc (ψ_2) and coefficient of power loss in the cycloid disc bearing (ψ_3).

$$\psi_{C_{loss}} = \psi_1 + \psi_2 + \psi_3 \tag{26}$$

The coefficient of power loss ψ_1 is defined by the expression:

$$\psi_1 = \frac{K_3 \cdot \mu_{ZO}}{z_2} \tag{27}$$

where: K_3 – factor accounting for the correction of the cycloid disc tooth [36,37]; μ_{ZO} – coefficient of sliding friction between the ring gear rollers and their pins [36,37].

The coefficient of power loss ψ_2 is given by the expression:

$$\psi_2 = \frac{30 \cdot P_{VK}}{T_3 \cdot \pi \cdot (n_{iz} - n_{ul})} \tag{28}$$

where: P_{VK} – the power lost due to friction in the contact between the output rollers and the cycloid disc, (W); T_3 – torque at the cycloid disc, (Nm).

The power loss lost due to friction in the contact between the output rollers and the cycloid disc is defined as:

$$P_{VK} = \frac{4 \cdot T_3}{\pi \cdot R_{0\,izl}} \cdot e \cdot \frac{\pi \cdot (n_{iz} - n_{ul})}{30} \cdot \mu_{VO} \tag{29}$$

where: $R_{0\,izl}$ – radius of the circle where the cycloid disc holes are placed, (mm); e – eccentricity, (mm); μ_{VO} – coefficient of friction between the output rollers and their pins.

The power loss ψ_3 is defined as:

$$\psi_3 = 1.25 \cdot \frac{T_{fc}}{T_3} \tag{30}$$

where: T_{fc} – friction torque in the bearing, (Nm).

The torque (T_{fc}) in the cycloid disc bearing is given by the expression [36,37]:

$$T_{fc} = 1.3 \cdot \frac{f_b}{1000} \cdot \left(1 + \frac{d_{CZ}}{d_{kt}}\right) \cdot \frac{1000 \cdot T_3}{r_1} \cdot \sqrt{1 + \left(\frac{4}{\pi} \cdot \frac{r_1}{R_{0\,izl}} - K_Y\right)^2} \tag{31}$$

where: f_b – lever arm of the rolling friction of the cycloid disc bearing (f_b=0.005 mm) [36]; d_{CZ} – inner diameter of the bearing, (mm); d_{kt} – diameter of the rolling body of the cycloid disc bearing, (mm); r_1 – the radius of the stationary circle, (mm); K_Y – factor accounting for the correction of the cycloid disc tooth [36,37].

5. VEHICLE DESIGN CHARACTERISTICS

Nowadays, commuting from home to work with a distance under 50 *km* is the most common form of driving. That is why, in this paper, the focus is placed on a small passenger vehicle intended for city driving. Some typical vehicle characteristics are given in Table 1.

Table 1. Vehicle design characteristics

Characteristics	Units	Value
Translational mass of the vehicle, $\boldsymbol{m_v}$	kg	850
Vehicle carrying capacity, $\boldsymbol{m_c}$	kg	350
Maximum speed, $\boldsymbol{v_{max}}$	km/h	150
Rolling resistance coefficient, $\boldsymbol{\mu_0}$	-	0.01
Frontal area of the vehicle, A_f	m^2	1.75
Aerodynamic drag coefficient, C_d	-	0.3
Effective radius (185/60 R14), r_{dyn}	m	0.281
Reducer efficiency, η_R	-	0.95
Motor efficiency, η_{em}	-	0.90

Based on the given vehicle characteristics, four motors with permanent magnets, manufactured by Dana TM4, marked as IPM 200-50-AH01 [38], were chosen. Their characteristics are shown in Fig. 9.

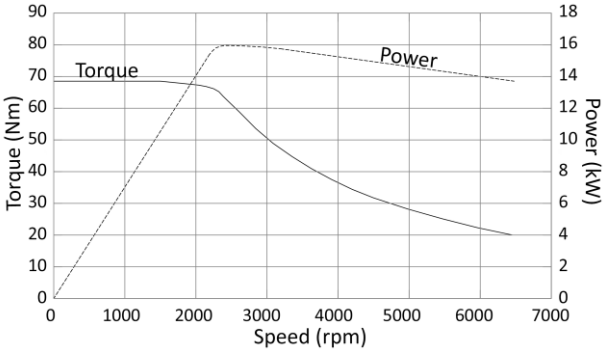

Fig. 9. Characteristics of the chosen motors [38]

Using the equations from section 3, values of the tractive effort and resistance as a function of the vehicle speed were determined. Here, the effect of the grading resistance is analysed for several different values of the longitudinal grade angle: 0° (0%), $\mathbf{5}$° (8.7%), $\mathbf{10}$° (17.6%), $\mathbf{15}$° (26.8%), $\mathbf{20}$° (36.4%), $\mathbf{25}$° (46.6%). The character of the change in the overall resistance to motion of the vehicle and the actual circumferential force hyperbola are shown in Fig. 10.

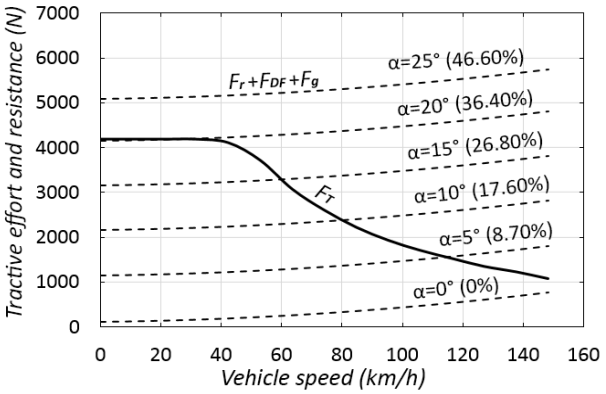

Fig. 10. Dependence of the tractive effort and the resistance on the current vehicle speed

Maximum speeds for different grade values are shown in Table 2.

Table 2. Dependence of the speed on the road grade angle

Angle, α (°)	Maximum speed of the vehicle, v (km/h)
0	150
5	116
10	80
15	60
20	30
25	0

The chosen motors with the given characteristics enable the vehicle to accelerate from 0 to 100 km/h in 13 s and to cover a distance of 219 m. The dependence between the acceleration time and the distance travelled is shown in Fig. 11.

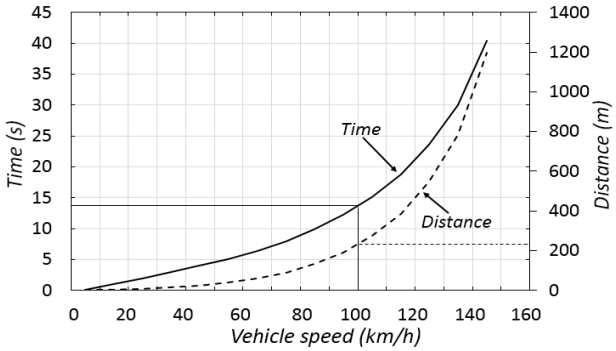

Fig. 11. Dependence of the acceleration time and distance travelled on the current vehicle speed

6. COMPARATIVE ANALYSIS OF PLANETARY AND CYCLOIDAL REDUCERS

In order to make an accurate comparison of the basic characteristics of planetary and cycloidal reducers in in-wheel-hub drive units, both reducers were designed to have the same operating characteristics which were determined according to the design characteristics of the vehicle and the WLTP cycle. They are presented in Table 3.

The value of the gear ratio of the reducer $u_R = 5$ was determined for the maximum vehicle speed and the maximum motor speed.

Table 3. Drive unit characteristics

Characteristics	Units	Value
Average torque, T_{em}	Nm	37.4
Average motor speed, n_{em}	min^{-1}	2195.1
Gear ratio of the reducer, u_R	-	5

The overall dimensions are one of the most important characteristics of a reducer. They are given in Fig. 12 and 13.

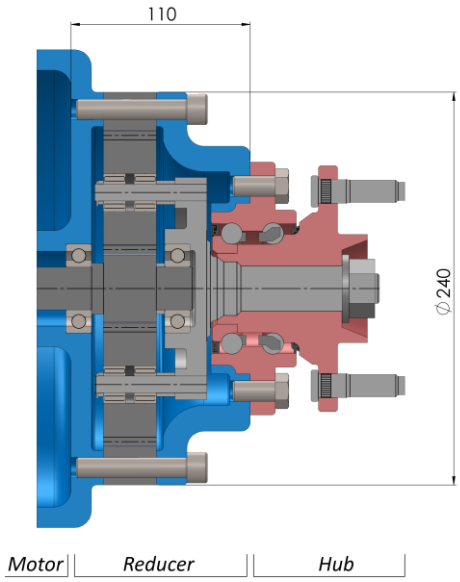

Fig. 12. Planetary in-wheel hub reducer, $u_R = 5$

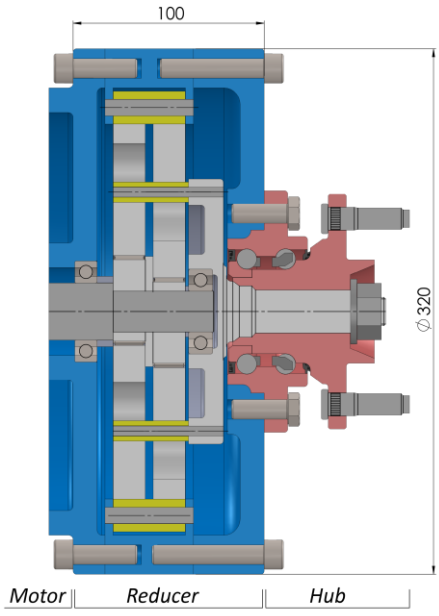

Fig. 13. Cycloidal in-wheel hub reducer, $u_R = 5$

The diameter of the cycloidal reducer is 25% larger than the diameter of the planetary reducer, while the length of the cycloidal reducer is 9.1% less compared to the planetary reducer. This means that planetary reducers have an advantage when a lower gear ratio ($\boldsymbol{u_R = 5}$) is needed, while at higher gear ratios, the advantage goes to cycloidal reducers because of a minimal increase in their dimensions.

The mass of the planetary reducer with the housing is 23.3 $\boldsymbol{kg}$, while the mass of the cycloidal reducer with the housing is 22.9 $\boldsymbol{kg}$, which is 1.7% less than the mass of the planetary reducer.

The efficiency of the planetary and cycloidal reducer was also determined following the procedure described in section 4.4. The values of the used friction coefficients and necessary factors are shown in Table 4

Table 4. The values of the used friction coefficients and factors

Characteristics	Units	Value
Coefficient of friction in the planet gear bearing, $\boldsymbol{\mu_b}$	-	0.0025
Factor accounting for the cycloid disc tooth correction, $\boldsymbol{K_3}$	-	1.62
Factor accounting for the cycloid disc tooth correction, $\boldsymbol{K_Y}$	-	0.223
Lever arm of the rolling resistance of the cycloid disc bearing, f_b	mm	0.005

Efficiency as a function of the current speed of the vehicle is shown in Fig. 14.

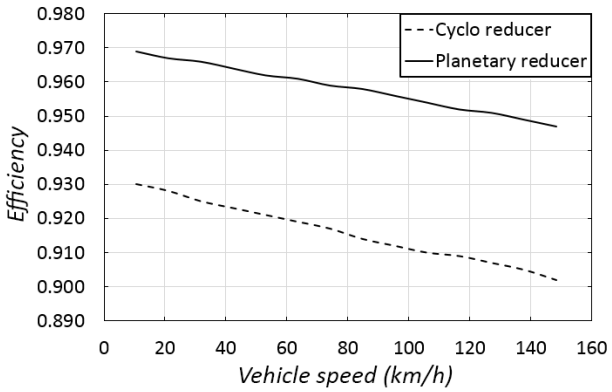

Fig. 14. Dependence of the efficiency on the current speed of the vehicle

The efficiency of the planetary reducer varies in the range of 0.969÷0.947 and has a tendency to decrease with the increase in the speed of the vehicle. The efficiency of the cycloidal reducer is 4÷5% lower and ranges between 0.930÷0.902 and also has a tendency to decrease with the increase in the vehicle speed.

This means that planetary reducers have an advantage in terms of efficiency at lower gear ratios, while cycloidal reducers have an advantage at higher gear ratios.

7. CONCLUSION

This paper describes possible design solutions for reducers in in-wheel hub drive units and gives a detailed analysis of main characteristics of single-stage planetary and cycloidal reducers.

In order to perform a comparative analysis, both types of reducers are designed for the same operating characteristics of an actual vehicle.

The results show that planetary reducers have an advantage in terms of dimensions and efficiency when a lower gear ratio is needed, such as $u_R = 5$, while cycloidal reducers have an advantage at higher gear ratios.

Our further research will include creation of a load spectrum based on which the exact value of the equivalent moment will be determined. A comparative analysis of reducers in terms of their reliability is also planned.

REFERENCES

[1] S. Cho, K. Ahn, J. M. Lee, Efficiency of the planetary gear hybrid powertrain. *Proceedings of the Institution of Mechanical Engineers, Part D: Journal of Automobile Engineering*, 220 (10), 2006: 1445-1454. https://doi.org/10.1243/09544070JAUTO176

[2] X. Ning, S. Zheng, W. Xie, Design principle of active load spectrum for shafting components in wheel hub reducer of electric vehicle. *Proceedings of the Institution of Mechanical Engineers, Part D: Journal of Automobile Engineering*, 233 (10), 2019: 2546-2558. https://doi.org/10.1177/0954407018800569

[3] A. Kulkarni, S. A Ranjha, A. Kapoor, A quarter-car suspension model for dynamic evaluations of an in-wheel electric vehicle. *Proceedings of the Institution of Mechanical Engineers, Part D: Journal of Automobile Engineering*, 232(9), 2018: 1139-1148. https://doi.org/10.1177/0954407017727165

[4] Y. Qin, C. He, P. Ding, M. Dong, Y. Huang, Suspension hybrid control for in-wheel motor driven electric vehicle with dynamic vibration absorbing structures. *IFAC-PapersOnLine*, 51(31), 2018: 973-978. https://doi.org/10.1016/j.ifacol.2018.10.054

[5] M. Bièek, T. Pepelnjak, F. Pušavec, Production aspect of direct drive in-wheel motors. *Procedia CIRP*, 81, 2019: 1278-1283. https://doi.org/10.1016/j.procir.2019.03.308

[6] J. Nerg, M. Rilla, V. Ruuskanen, J. Pyrhönen, S. Ruotsalainen, Design and drive-cycle based analysis of direct-driven permanent magnet synchronous machine for a small urban use electric vehicle. *IEEE Transactions on Industrial Electronics*, 61(8), 2014: 4286-4294. https://doi.org/10.1109/TIE.2013.2248340

[7] J. Li, C. Han, W. Wu, T. Tang, X. Ran, Z. Zheng, S. Sun, Load Spectrum Compilation Method of Hybrid Electric Vehicle Reducers Based on Multi-Criteria Decision Making. *Energies*, 15(9), 2022: 3293. https://doi.org/10.3390/en15093293

[8] Y. Kaneko, H. Hirano, K. Shishido, K. Asogawa, Development of compact and high output In-Wheel-Motor unit. *Review of Automotive Engineering Final*, 31, 2010: 140-143. https://doi.org/10.11351/jsaereview.31.140

[9] S. Murata, Innovation by in-wheel-motor drive unit. *Vehicle System Dynamics*, 50(6), 2012: 807-830. https://doi.org/10.1080/00423114.2012.666354

[10] I. Petrov, J. Pyrhonen, Performance of low-cost permanent magnet material in PM synchronous machines. *IEEE Transactions on Industrial Electronics*, 60(6), 2012: 2131-2138. https://doi.org/10.1109/TIE.2012.2191757

[11] A. Flodin, B. Kianian, Tesla teardown: Identifying potential uses for PM in electric vehicle transmissions. *Powder Metallurgy (PM) Gear Manufacturing*, 10(4), 2021: 45-52.

[12] R. Mizutani, F. Kurata, S. Yogo, K. Harada, A. Torii, Y. Tojima, M. Sakuma, Toyota Motor Corp, Aisin Corp, In-Wheel motor with high durability, US patent US20060144626A1, published 2006-07-06.

[13] K.H. Shin, Hyundai Mobis Co Ltd, In-wheel working device, US patent US20180118022A1, published 2018-05-03.

[14] T. Makino, NTN Corp, Cycloidal speed reducer, in-wheel motor drive device, and vehicle motor drive device, US patent US20110082000A1, published 2011-04-07.

[15] M. Suzuki, K. Yamamoto, R. Yukishima, NTN Corp, In-wheel motor-driven device, US patent US9302578B2, published 2015-01-22.

[16] X.X. Sun, L. Han, A new numerical force analysis method of CBR reducer with tooth modification. *Journal of Physics: Conference Series*, 1187(3), 2019: 032053. https://doi:10.1088/1742-6596/1187/3/032053

[17] Z. Xu, W. Yu, Y. Shao, Dynamic modeling of the planetary gear set considering the effects of positioning errors on the mesh position and the corner contact. *Nonlinear Dynamics*, 109(3), 2022: 1551-1569. https://doi.org/10.1007/s11071-022-07570-9

[18] M. Blagojevic, M. Matejic, N. Kostic, Dynamic Behaviour of a Two-Stage Cycloidal Speed Reducer of a New Design Concept. *Technical Gazette*, 25(2), 2018: 291-298. https://doi.org/10.17559/TV-20160530144431

[19] J. Wang, Y. Wang, Z. Huo, Finite Element Residual Stress Analysis of Planetary Gear Tooth. *Advances in Mechanical Engineering*, 5, 2013: 761957. https://doi.org/10.1155/2013/761957

[20] M. Blagojevic, N. Marjanovic, Z. Đordevic, B. Stojanovic, A. Dišic, A New Design of a Two-Stage Cycloidal Speed Reducer. *Journal of Mechanical Design*, 133(8), 2011: 085001-1 - 085001-7. https://doi.org/10.1115/1.4004540

[21] F. Concil, Thermal and efficiency characterization of a low-backlash planetary gearbox: An integrated numerical-analytical prediction model and its experimental validation. *Proceedings of the Institution of Mechanical Engineers, Part J: Journal of Engineering Tribology*, 230(8), 2016: 996-1005. https://doi.org/10.1177/1350650115622363

[22] K. Olejarczyk, M. Wiklo, K. Kolodziejczyk, The cycloidal gearbox efficiency for different types of bearings—Sleeves vs. needle bearings. *Proceedings of the Institution of Mechanical Engineers, Part C: Journal of Mechanical Engineering Science*, 233(21-22), 2019: 7401-7411. https://doi.org/10.1177/0954406219859903

[23] C.M.C.G. Fernandes, P.M.T. Marques, R.C. Martins, J.H.O. Seabra, Gearbox power loss. Part III: Application to a parallel axis and a planetary gearbox. *Tribology International*, 88, 2015: 317-326. https://doi.org/10.1016/j.triboint.2015.03.029

[24] M. Vasic, M. Blagojevic, M. V. Dragoi, Thermal stability of lubricants in cycloidal reducers. *Engineering Today*, 1(2), 2022: 7-17. https://doi.org/10.5937/engtoday2202007V

[25] H. Naunheimer, B. Bertsche, J. Ryborz, W. Novak, Automotive Transmissions. *Springer*, Berlin, 2011.

https://doi.org/10.1007/978-3-642-16214-5
[26] G. Sieklucki, Optimization of Powertrain in EV. *Energies*, 14(3), 2021: 725. http://dx.doi.org/10.3390/en14030725
[27] P.D. Walker, S.A. Rahman, N. Zhang, Modelling, simulations, and optimisation of electric vehicles for analysis of transmission ratio selection. *Advances in Mechanical Engineering*, 5, 2013: 340435. http://dx.doi.org/10.1155/2013/340435
[28] B. Gao, Q. Liang, Y. Xiang, L. Guo, H. Chen, Gear ratio optimization and shift control of 2-speed I-AMT in electric vehicle. *Mechanical Systems and Signal Processing*, 50-51: 2015, 615-631. https://doi.org/10.1016/j.ymssp.2014.05.045
[29] A.D. Pham, H.J. Ahn, High precision reducers for industrial robots driving 4th industrial revolution: state of arts, analysis, design, performance evaluation and perspective. *International Journal of Precision Engineering and Manufacturing-Green Technology*, 5(4), 2018: 519-533. http://dx.doi.org/10.1007/s40684-018-0058-x
[30] Sumitomo, Cyclo 6000 Reducer Catalog. *Sumitomo Machinery Corporation of America*, USE, 2015.
[31] M. Tutuianu, A. Moratta, H. Steven, E. Ericsson, T. Haniu, N. Ichikawa, H. Ishii, Development of a World-wide Worldwide harmonized Light duty driving Test Cycle (WLTC), Techical Report. *68th GRPE,* 2014.
[32] ISO 6336-6:2019 - Calculation of load capacity of spur and helical gears - Part 6: Calculation of service life under variable load
[33] Precision Reduction Gear RV Catalogue. *Nabtesco*, 2018.
[34] S. Tanasijevic, Mechanical transmissions (in Serbian). *Faculty of Engineering University of Kragujevac*, Kragujevac, 2006.
[35] M. Blagojevic, Kinematic and dynamic analysis of single - stage cyclo speed reducer (Master's Thesis, in Serbian). *Faculty of Engineering University of Kragujevac*, Kragujevac, 2003.
[36] V.N. Kudryavcev, Planetarnye peredachi. *Masinostroenie*, Moskva, 1966. (In Russian)
[37] M. Vasic, M. Matejic, M. Blagojevic, A comparative calculation of cycloid drive efficiency. *Conference on Mechanical Engineering Technologies and Application-COMETA*, East Sarajevo (SR BiH), 2020: 259-266.
[38] IPM 200 series catalogue - Internal Permanent Magnet Motors. *Dana TM4 Inc*, 2020.